Original Article

Multi-Parametric MR Image Registration in Glioma Brain Tumors Using Multi-Similarity (RC and NMI) Measures Based on Wavelet Transform

Mojtaba Safari[1,2], Anahita Fathi Kazerooni[1,2], Hamidreza Saligheh Rad[1,2*]

1- Quantitative MR Imaging and Spectroscopy Group (QMISG), Research Center for Molecular and Cellular Imaging, Tehran University of Medical Sciences, Tehran, Iran.

2- Department of Medical Physics and Biomedical Engineering, Tehran University of Medical Sciences, Tehran, Iran.

Received: 3 September 2017
Accepted: 10 November 2017

Keywords:
Multi-Parametric Magnetic Resonance Imaging,
Registration,
Brain Tumors,
Similarity Measure,
Wavelet Pyramid.

ABSTRACT

Purpose- The objective of this study is to align multi-parametric MR images of brain tumors using the wavelet transformation and multi-similarity (RC and NMI) measures.

Materials and Methods- In this work, we implemented a 2D multi-level non-rigid registration technique with multi-similarity measures for the registration of perfusion and diffusion–derived (rCBV and ADC) maps to morphological FLAIR images. To evaluate the performance of our proposed algorithm, we used synthetic data to test the robustness of the method to noise and intensity inhomogeneity. Finally, the algorithm was applied to multiparametric images (FLAIR/rCBV-/ADC-maps) of 10 patients with glial tumors.

Results- The evaluation of the proposed method on synthetic and real data revealed that this approach has a large capture range and is robust against noise and intensity inhomogeneity without increasing the load and complexity of registration algorithm. The results for synthetic data contaminated with noise and intensity inhomogeneity based on Hausdorff Distance (HD), Root Mean Square Error (RMSE) and Baddeley's delta image metric (Δ) improved by 8%, 8% and 21% respectively. For real data, the overall performances based on RMSE and HD metrics were 28% and 10% for ADC-map to FLAIR registration, and 40% and 14% for rCBV-map to FLAIR registration.

Conclusion- In this work, through the proposed multi-similarity measure combined with each other in different wavelet decomposition levels, we showed that the capture range of multiparametric image registration algorithm, robustness against noise, and intensity inhomogeneity artifacts could be improved.

1. Introduction

Multi-parametric MR image registration of glioma brain tumors is an essential procedure through which physiological maps derived from quantitative MR imaging techniques, such as Diffusion-Weighted Imaging (DWI) and Perfusion-Weighted Imaging (PWI) using Dynamic Susceptibility Contrast-Enhanced (DSC-) MRI, are aligned with anatomical MR images. In this context, image registration, as a pre-processing step, has close associations with the accuracy of the consequent quantification steps such as

Corresponding Author:
Hamidreza Saligheh Rad, PhD
Quantitative Medical Imaging Systems Groups, Medical Physics and Biomedical Engineering Department, Tehran University of Medical Sciences, Tehran, Iran.
Tel: (+98) 2188973653 – 108, Fax: (+98) 2166466383.
E-mail: h-salighehrad@tums.ac.ir

multi-parametric MR image combination [1], segmentation of the subregions within brain tumors [2, 3], computer-aided diagnosis [4], and longitudinal studies for treatment response follow-up [5] which are highly dependent on it.

Multi-parametric image registration is desirable as each modality contains a specific property; for example, conventional or anatomical MR images like T1 and T2-weighted or Fluid Attenuated Inversion Recovery (FLAIR) images exhibit a high spatial resolution. Unlike anatomical MR images, physiological images and quantitative maps, such as DWI and its derived Apparent Diffusion Coefficient (ADC) map which represent cellular distribution within the tissue, or DSC-MRI and its derived regional Cerebral Blood Volume (rCBV) map which represent the changes in blood perfusion and tumor neo-angiogenesis, lack accurate anatomical structures and usually have larger voxel sizes than conventional images. To achieve an accurate diagnosis and treatment planning outcome, maintaining both spatial and contrast resolution are necessary, highlighting the importance of multi-parametric image registration [6-9].

Medical image registration framework usually consists of three major steps for aligning a source to a reference image: Similarity Measure (SM), transformation, and optimization [10]. The initial step is to align images through finding counterpart pixels or voxels in the reference and source images by applying a similarity measure. The next steps are transformation and optimization, in which the corresponding pixels or voxels are being transformed to each other optimally.

Image registration is mathematically defined as:

$$\hat{\theta} = arg_{\theta} min\{\psi(\theta)\} \quad (1)$$

where $\psi(\theta)$ is SM, θ is the vector of parameters of the transformation, and the aim is to find the best θ that minimizes the dissimilarity between the source and reference images.

There are several ways to categorize medical image registration techniques, e.g. based on the type of transformation including rigid or non-rigid body transformations, or different SMs, such as intensity or information based SM [10-12]. Rigid body transformation can only rotate and translate the images to be registered while through non-rigid registration, any type of deformation may be employed to align the images with each other [7]. Affine transformation is the simplest form of non-rigid body transformation that can rotate, translate and scale the images [13, 14].

SMs can be classified into two broad categories including (1) intensity-based methods that define similarity of two images solely based on their intensity values, and (2) information theory-based SMs that define the similarity based on Mutual Information (MI) of two images [15, 16]. Intensity-based SMs are used when alignment of mono-modal images is desired. However, for multi-modal or multi-parametric image registration schemes, information-based SMs must be employed.

In this work, our aim is to propose an approach to align the quantitative ADC and rCBV maps to anatomical FLAIR images with high accuracy and low computational burden. The selected set of multi-parametric images including FLAIR, ADC-map, rCBV-map in this study has shown to produce the necessary information for the discrimination of glioma brain tumor subregions (2).

2. Materials and Methods

We propose a multi similarity measure (multi-SM) method to reduce the sensitivity to bias field and white Gaussian noise in the MR images and multi-level image registration method, through a wavelet pyramid to increase the capture range [8]. For multi-SM method, we use the Residual Complexity (RC) and MI similarity measures [9, 17]. RC measure helps to compensate for the existing noise and bias field artifacts. Furthermore, we use non-rigid transformation with spline basis function due to its smoothness and being twice differentiable [11, 12, 18-20]. Here, the efficacy of the proposed algorithm is first tested and optimized on synthetic data and then applied to real data, which consists of MR images of patients with glioma brain tumors. The whole procedure was implemented in MATLAB 2016a (MathWorks Inc).

2.1. Generation of Synthetic Data

Our 2D synthetic data was created by using two logical circles with radii of 50 pixels; one of them being reshaped by the following transformation:

$$u = x_i + 5 * sin\left(\frac{\pi x_i}{128}\right) + 2 * sin\left(\frac{2\pi x_i}{128}\right)$$

$$v = y_i + 3 * sin\left(\frac{\pi y_i}{128}\right) + 7 * sin\left(\frac{2\pi y_i}{128}\right) \quad (2)$$

To evaluate the performance of our approach in the presence of noise, we corrupted the synthetic data by white Gaussian noise with a different Contrast to Noise Ratios (CNR). White Gaussian noise was selected due to its similarity to the noise corrupting the real MR images. The assessment of robustness of the registration algorithm against bias field (intensity inhomogeneity) distortion was performed by adding a multi-modal Gaussian function to the images to imitate intensity inhomogeneity, as described below:

$$I_{after}(x,y) = I_{before}(x,y) + \frac{1}{K}\sum_{k=1}^{K} e^{-\frac{\|[x;y]-\mu_k\|^2}{2\sigma^2}} \quad (3)$$

where I_{before} is the clean image, without adding bias field (intensity inhomogeneity) artifact, I_{before} is the distorted image, and k is the number of the Guassian modes to corrupt the images with bias field inhomogeneity artifact, and μ_k,σ are the mean and standard deviation of the added Gaussian function, respectively. Here, we selected $k=2$, and $\sigma=30$ and $\mu_1=(168,80)$,$\mu_2=(179,127)$. The flowchart of generating the deformed and corrupted synthetic data is shown in Figure 1 and the synthetic data are shown in Figure 2.

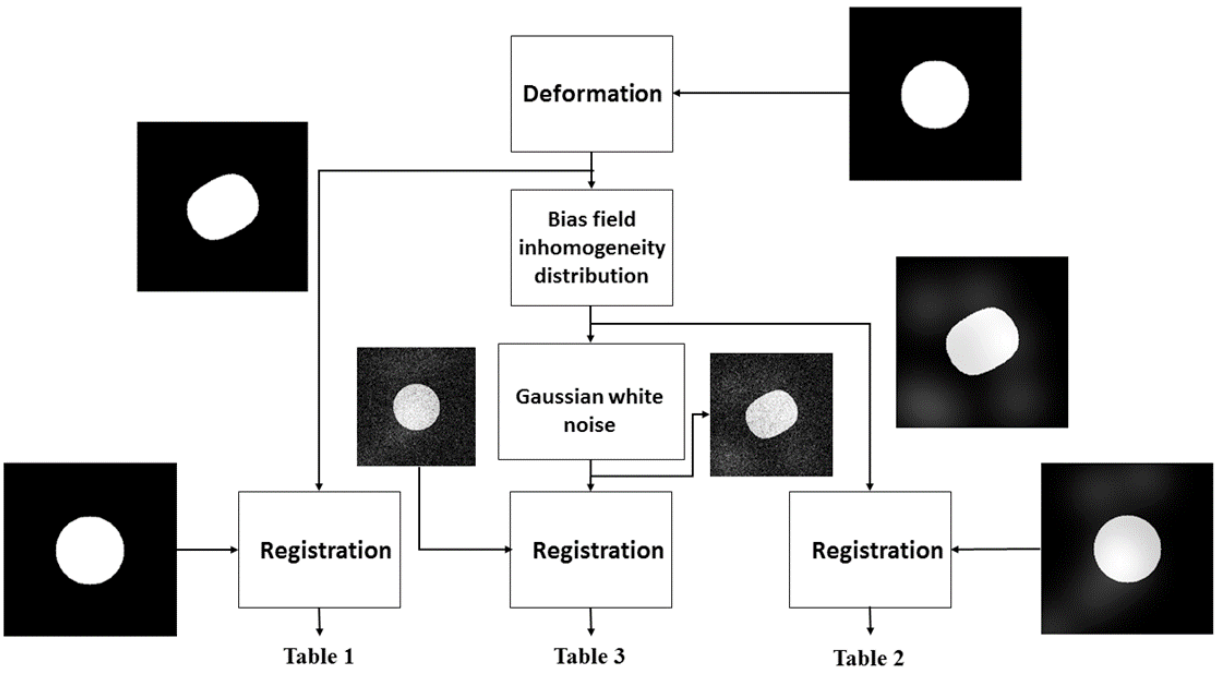

Figure 1. The flowchart of generating distorted synthetic data and evaluating the performance of the proposed registration method on this synthetic data which is tabulated in Tables 1 to 3.

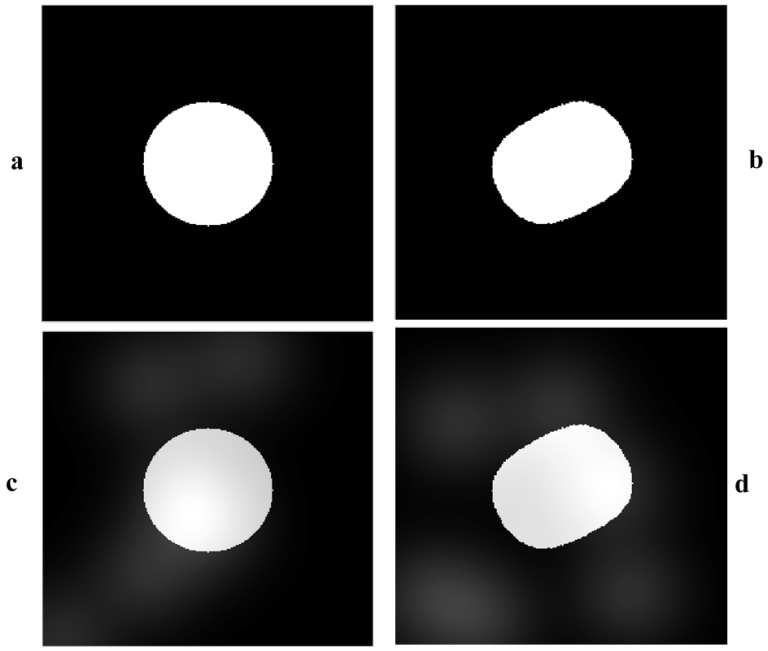

Figure 2. Synthetic data, a) a circle with 50-pixel radius, b) transformed form of synthetic data in *a*, c) intensity inhomogeneity distortion added to *a*, and d) intensity inhomogeneity distortion added to transformed image.

2.2. Characteristics of Real Data

In this study, we used MR images (FLAIR, ADC-map, rCBV-map) of 10 patients diagnosed with glioma brain tumors. The details about histopathological diagnosis of the patients, MR image acquisition and the quantification technique for the generation of rCBV maps can be found elsewhere [1]. An example of a set of multi-parametric images for a patient diagnosed with grade II Oligoastrocytoma is indicated in Figure 3.

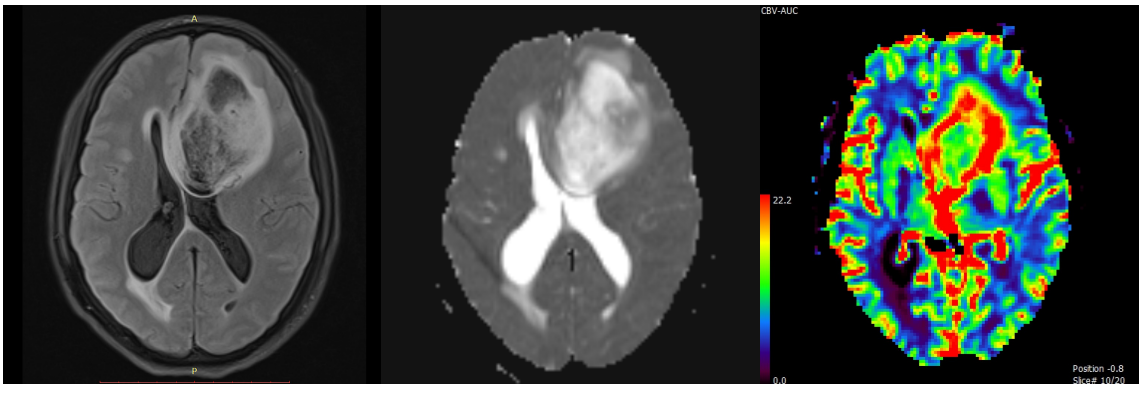

(A) (B) (C)

Figure 3. An example of a set of multi-parametric images of a patient histopathologically diagnosed with grade 2 Oligoastrocytoma: (A) T2-FLAIR image, as the reference or fixed image for registration; (B) ADC-map, as the source or moving image for registration; (B) color-coded rCBV-map, as the source or moving image for registration.

2.3. The Proposed Registration Framework

2.3.1. General Scheme

The proposed 2D multi-SM registration framework takes advantage of the capabilities of both intensity based (RC) and information theory based (MI) similarity measures, to increase the robustness against noise and intensity inhomogeneity disruptions. To prevent the algorithm from falling into the trap of local minima and to increase the optimization speed, we used multi-level pyramid of images for the image registration. The pyramid of images was created by using wavelet transform with Haar basis function [21]. A typical choice for creating multi-level pyramid of images is to use the Gaussian pyramid. Here, wavelet transform was used instead of Gaussian pyramid to increase the accuracy of registration as wavelet transform creates less blurry than the Gaussian pyramid [8]. These two types of pyramids are shown in Figure 4. Wavelet transform decomposes the images into four sub-band images labeled as LL (Low-Low), HL (High-Low), LH (Low-High) and HH (High-High). In this work, we used LL sub-band coefficient to perform image registration. We used spline-based interpolation and transformation because of its smoothness and being twice differentiable which is important for optimization.

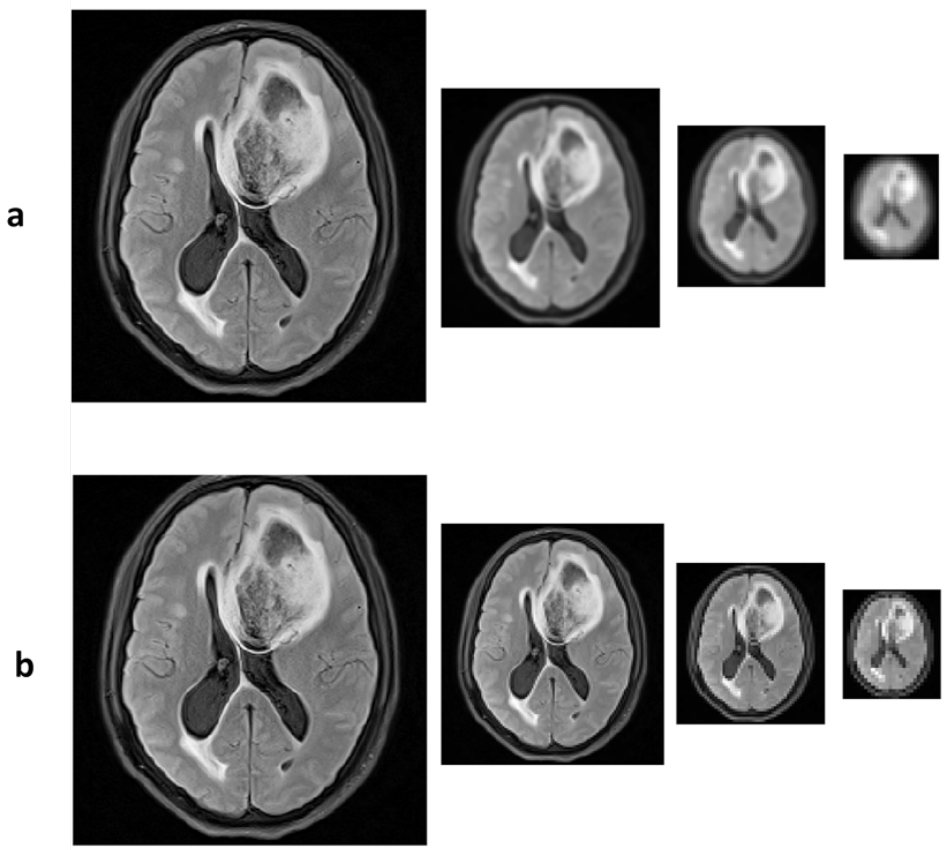

Figure 4. Pyramid of FLAIR image, a) Gaussian pyramid and b) wavelet pyramid. Wavelet pyramid preserves more spatial information than Gaussian pyramid.

2.3.2. The Proposed Multi-Similarity Measure

Similarity measure is one of the key components of image registration and is optimized when the correct spatial alignment between the two images is achieved. Intensity-based SMs work directly on the intensity of images and usually rely on the assumption that neighboring pixels are independent from each other [17]. Examples of such intensity-based SMs are Sum-of-Squared-Differences (SSD), Correlation Coefficient (CC), Correlation Ratio (CR), and Sum-of-Squared-Differences (SSD) which are defined between corresponding pixels in the source and the reference images without considering their spatial dependencies.

Nonetheless, MR images which are acquired at higher magnetic fields (e.g. 3T) are often corrupted by slowly-varying bias fields, i.e. intensity inhomogeneity. The assumption of the independency of the adjacent pixels within an MR image becomes invalidated by intensity inhomogeneity. As a result, the aforementioned similarity measures tend to fail in aligning the images.

To reduce the effects of the bias field, three main approaches have been proposed:

1. Bias field correction methods can be applied to the images prior to registration [22]; this approach cannot be employed in our problem because of the quantitative nature of ADC and rCBV maps, when quantitative measurements become erroneous after the application of bias field correction methods.

2. Block-wise registration method can be implemented without applying any changes to the employed SMs; this approach imposes huge a calculation time and increases the possibility of getting into the trap of local minima.

3. SMs with robustness to slowly-varying intensity inhomogeneity such as Residual-Complexity(RC) [9, 17] similarity measure can be exploited.

The cost function for RC similarity measure can be defined as follows:

$$E(\tau) = \sum_{n=1}^{N} log\left(\frac{(q_i^T r)^2}{\alpha} + 1\right) \quad (4)$$

where is the constant trading parameter and r is the difference of the fixed (reference) image (I) and the moving (source) image (J^T):

$$r = I - J^T \quad (5)$$

Intuitively, when two images are aligned in correct coordinates, they must have low complexity and the residual image must be sparse. Therefore, we used $log(x^2 + 1)$ to represent the quantitative sparseness of x that in here $x = q_i^T r / \sqrt{\alpha}$. $q_i^T r$ is the measure of complexity of the residual image (r). The basis functions used here are Discrete Cosine Transform (DCT) of residual image.

Although RC similarity measure has the advantage of accounting for spatial intensity inhomogeneity, it is a mono-modal similarity measure and does not work properly for multi-modal or multi-parametric image registration of brain tumors. To take advantage of RC capture range, we used RC similarity measure in the lower levels of pyramid images. In high levels, we used the Normalized Mutual Information (NMI) similarity measure [15, 16] as a multi-modal/multi-parametric similarity measure. NMI is mathematically described as follows:

$$E_{NMI}(\tau) = \frac{H(I) + H(J^\tau)}{H(I, J^\tau)} \quad (6)$$

where H(•) and H(•,•) are the entropy and joint entropy, respectively. Entropy and joint entropy of images are mathematically presented with:

$$H(I) = -\sum_i p(i) \times \log_2\{p(i)\} \quad (7)$$

$$H(I, J^\tau) = -\sum_i \sum_j p(i, j) \times \log_2\{p(i, j)\} \quad (8)$$

where $p(i)$ is the probability of occurrence of each pixel calculated by dividing the intensity of each pixel by the number of all pixels; $p(i, j)$ is the joint probability of images which is calculated from the joint histogram of two images [11, 12, 23, 24].

2.3.3. Transformation Function and Optimization

We used B-spline transformation function to align the images [18, 25]. B-spline is smoothly-varying and twice differentiable, as described below:

$$T_\theta(x) = x + \sum_{x_k \in N_x} \theta_k \beta^3\left(\frac{x - x_k}{s}\right) \quad (9)$$

where θ_k is the k^{th} parameter of transformation, $\beta^3(x)$ is the third-order B-spline polynomial defined by [19]:

$$\beta^3(x) = \begin{cases} \frac{2}{3} - |x|^2 + \frac{|x|^3}{3}, & 0 \le |x| \le 1 \\ \frac{(2 - |x|)^3}{6}, & 1 \le |x| \le 2 \\ 0, & 2 \le |x| \end{cases} \quad (10)$$

N_x is the set of all control points (x_k) within the compact support of the B-spline at point x.

To optimize the cost function, we used Broyden–Fletcher–Goldfarb–Shanno (BFGS) method, described by the following equation :

$$\theta_{k+1} = \theta_k - \lambda_k (\nabla^2 \psi(\theta_k) + \mu_k I)^{-1} \nabla \psi(\theta_k)$$

where ψ is the cost function defined based on the similarity measures and $\nabla^2 \psi(\theta_k)$ is the Hessian matrix of cost function. Hessian matrix in this optimization scheme has low computational time [26].

2.3.4. Evaluation Metrics

For the quantitative assessment of the results of registration of synthetic data, we used three kinds of metrics including Baddeley's delta image metric (Δ) [27], Hausdorff Distance (HD) [28, 29] and Root-Mean-Square-Error (RMSE) [30].

Baddeley's delta image metric (Δ) is used for binary images and takes the spatial information of images. This metric intuitively works very well and is defined below:

$$\Delta_w^p(A,B) = \left\{ \frac{1}{N} \sum_{x \in X} \left| w[d(x,A)] - w[d(x,B)] \right|^p \right\}^{1/p} \quad (11)$$

where N is number of pixel and X is the raster image A and image B. w is the convex continuous function which is strictly increasing in zero: $w(z) = \min\{z, c\}$, and c is the constant. p is the norm. When $p=1$, Δ is the geometrical average and also if $p=2$, Δ is the Euclidean norm. In our work, we used $p=2$ and $c=1$, the distance between pixels are less than one. As a result of Δ, images are more similar if Δ tends more in small number, two images are alike if $\Delta=0$.

Hausdorff Distance (HD) measures how much two data sets are far from each other. These two datasets in our work are fixed and floating images. This metric is mathematically defined as follows:

$$H(A,B) = \max(h(A,B), h(B,A)) \longrightarrow h(A,B) = \max_{a \in A} \min_{b \in B} \| a - b \| \quad (12)$$

where H is the Hausdorff Distance. Intuitively, $h(A, B)$ finds the minimum distance between points in A and B, which this point, a, in set A has the maximum distance from other point in this set, A, and H searches this approach for two sets separately and finds the maximum distance between these two sets.

Root-Mean-Square-Error (RMSE) measures the standard deviation error between fixed and floating images and is defined as:

$$RMSE = \sqrt{\frac{1}{n} \sum_{i=1}^{n} (r_i)^2} \longrightarrow r_i = I_{moving}(\tau_{\hat{\theta}}(x_i)) - I_{moving}(x_i) \quad (13)$$

3. Results

3.1. Synthetic Data

The results of registration for clean synthetic data, synthetic data corrupted with intensity inhomogeneity artifact, and synthetic data corrupted with both Gaussian noise and bias field inhomogeneity are tabulated in Table 1-3, respectively. As mentioned earlier, to check the performance of our proposed multi-similarity (RC/NMI) measure in comparison with MI, NMI, and RC/MI metrics against the intensity inhomogeneity distortion and White Gaussian noise, we used three steps on three variations of synthetic data. At first, we created synthetic data and deformed it geometrically by Equation 2. The evaluation results of these images are indicated in Table 1.

Table1. Assessment of different metrics in the registration of clean synthetic data in terms of HD, RMSE, and Δ metrics.

	MI	NMI	RC/MI	RC/NMI
HD	4.35	3.50	1.98	1.69
RMSE	0.041	0.032	0.007	0.004
Δ	8.75	6.95	0.91	0.66

As it can be observed, our proposed multi-similarity measure has the best overall performance in comparison with MI, NMI, or RC/MI measures. Without noise and intensity inhomogeneity artifacts, RC similarity measure works just like SSD similarity measure and also NMI can compensate for geometrical distortion of the two images.

Table2. Assessment of different metrics in the registration of synthetic data corrupted with intensity inhomogeneity artifact in terms of HD, RMSE, and Δ metrics.

SM Metric	MI	NMI	RC/MI	RC/NMI
HD	3.39	3.39	1.74	1.64
RMSE	0.08	0.07	0.06	0.06
Δ	0.8	0.8	0.83	0.83

In the next step, we added intensity inhomogeneity artifact, as described in Equation 3, and checked the performance of our approach. Our multi-similarity measure tends to return better results according to all evaluation metrics, except for Δ metric; but overall, our approach is more robust than other measures against intensity inhomogeneity.

Finally, we added white Gaussian noise to the images. The noise was applied with different levels of CNR and the results of this step is shown in Table 3. As HD metric is highly sensitive to noise itself; HD in noisy data tends to fail but other metrics show better performances against noise. Our approach in this synthetic data showed a higher performance than other similarity metrics and these results suggest that our approach produces accurate results after the registration.

Table 3. Assessment of different metrics in the registration of synthetic data corrupted with white Gaussian noise and intensity inhomogeneity artifacts with different levels of CNRs and in terms of HD, RMSE, and Δ metrics.

CNR(dB)	SM Metric	MI	NMI	RC/MI	RC/NMI
17.54	HD	2.82	2.60	4.53	4.27
	RMSE	0.08	0.09	0.12	0.12
	Δ	1.5	1.5	0.54	0.54
4.92	HD	3.6	3.67	4.23	4.20
	RMSE	0.14	0.15	0.17	0.17
	Δ	0.98	0.98	0.61	0.61
1.80	HD	4.55	4.60	5.11	5.03
	RMSE	0.19	0.20	0.21	0.22
	Δ	0.67	0.67	0.63	0.62
0.80	HD	5.72	5.70	6.20	6.16
	RMSE	0.25	0.25	0.27	0.27
	Δ	0.82	0.82	0.65	0.65

3.2. Real Data

As mentioned before, the proposed registration method has a larger capture range than other similarity metrics. For quantitative evaluation and comparison of the capture range of the registration metrics, we translated image pixels of each slice in 11 steps and in each step, we translated 3 pixels. Through this method, as shown in Figure 5, the capture range for RC/NMI metric is high and generates more accurate results than MI, NMI, or RC/MI metrics. The results of the registration of ADC- and rCBV-maps to FLAIR images are indicated in Table 4-5, respectively.

Table 4. Assessment results of ADC-map to FLAIR image registration.

SM Patients	Metric	MI	NMI	RC/MI	RC/NMI
CASE 1	RMSE	0.1140	0.1230	0.1024	0.0842
	HD	2.6193	2.7603	2.4299	2.4381
CASE 2	RMSE	0.1421	0.1277	0.1032	0.0923
	HD	2.7763	2.7939	2.5076	2.3326
CASE 3	RMSE	0.1435	0.1060	0.1042	0.0842
	HD	2.4268	2.4483	2.5451	2.2937
CASE 4	RMSE	0.1240	0.1203	0.1099	0.0929
	HD	2.6409	2.6520	2.2128	2.3459
CASE 5	RMSE	0.1261	0.1338	0.1024	0.0821
	HD	2.6158	2.4770	2.2494	2.1822
CASE 6	RMSE	0.1202	0.1130	0.1085	0.0953
	HD	2.4371	2.6541	2.3127	2.3154
CASE 7	RMSE	0.1466	0.1330	0.1028	0.0828
	HD	2.6343	2.5781	2.2496	2.2961
CASE 8	RMSE	0.1263	0.1163	0.1173	0.0897
	HD	2.5281	2.4838	2.4260	2.3561
CASE 9	RMSE	0.1371	0.1158	0.1045	0.0830
	HD	2.7992	2.4328	2.2423	2.1568
CASE 10	RMSE	0.1022	0.1247	0.1029	0.0888
	HD	2.6495	2.4208	2.5785	2.3915
Mean ∓ STD	RMSE	0.1282 ∓ 0.0142	0.1214 ∓ 0.0089	0.1058 ∓ 0.0048	0.0875 ∓ 0.0049
	HD	2.6127 ∓ 0.1233	2.5701 ∓ 0.1383	2.3754 ∓ 0.1386	2.3108 ∓ 0.0864

Table 5. Assessment results of rCBV-map to FLAIR image registration.

SM Patients	Metric	MI	NMI	RC/MI	RC/NMI
CASE 1	RMSE	0.1203	0.1237	0.0898	0.0938
	HD	2.6162	2.0094	2.3560	1.7521
CASE 2	RMSE	0.1147	0.1246	0.0882	0.0841
	HD	2.2905	1.9473	2.0364	1.7102
CASE 3	RMSE	0.1134	0.1048	0.094	0.0889
	HD	2.0522	1.9677	1.0743	1.6630
CASE 4	RMSE	0.1686	0.1668	0.0917	0.0762
	HD	2.2440	1.9382	2.0234	1.7256
CASE 5	RMSE	0.1194	0.1048	0.0898	0.0757
	HD	2.2545	1.9359	2.0283	1.6025
CASE 6	RMSE	0.1213	0.1011	0.0973	0.0829
	HD	2.2673	2.1185	1.0986	1.7296
CASE 7	RMSE	0.2163	0.2126	0.0935	0.0983
	HD	2.0720	2.0463	1.0953	1.5889
CASE 8	RMSE	0.1227	0.1146	0.929	0.1063
	HD	2.1505	2.0389	2.0364	1.6063
CASE 9	RMSE	0.1084	0.1107	0.0978	0.0776
	HD	2.1157	1.9383	2.0173	1.9235
CASE 10	RMSE	0.2746	0.2739	0.0888	0.0889
	HD	2.2502	2.1144	2.1650	1.8267
Mean ∓ STD	RMSE	0.1480 ∓ 0.0575	0.1438 ∓ 0.0575	0.1760 ∓ 0.2646	0.087 ∓ 30.0101
	HD	2.2313 ∓ 0.1603	2.005 ∓ 0.0716	1.7931 ∓ 0.4964	1.7128 ∓ 0.1058

According to the error bars shown in Figure 6, our proposed approach returns higher accuracy in comparison to other conventional metrics, and does not impose additional computational burden. As it can be observed in Figure 4, RC similarity measure also generates optimum results but it does not have high capture range as our proposed RC/NMI similarity measure. This high capture range highly depends on wavelet pyramid because wavelet pyramid creates less blurry images than Gaussian pyramid, so it contains more spatial information of the brain.

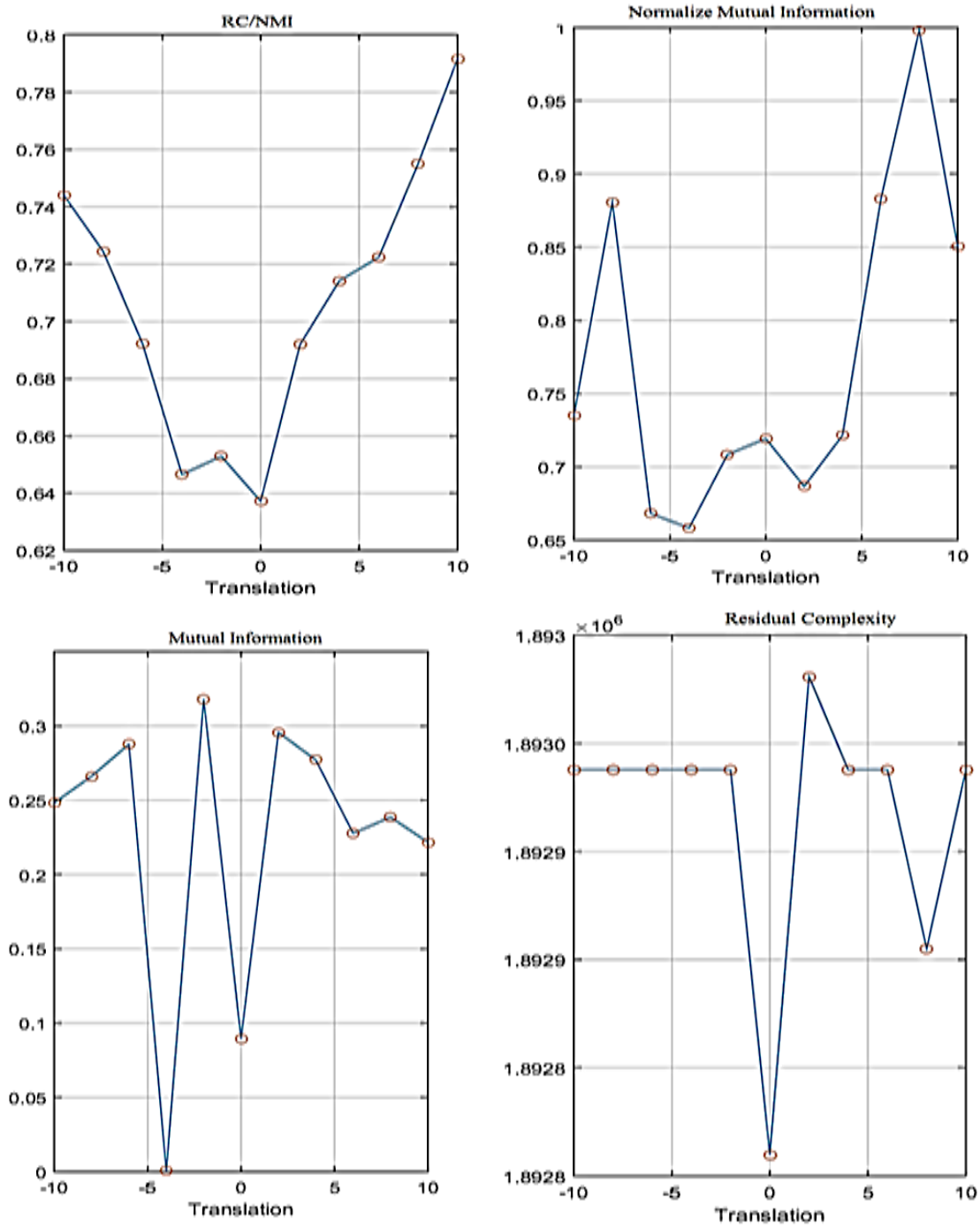

Figure 5. Show the change of similarity measure with the translation of float image that show the capture rang of RC/NMI is high and reaches the global minimum.

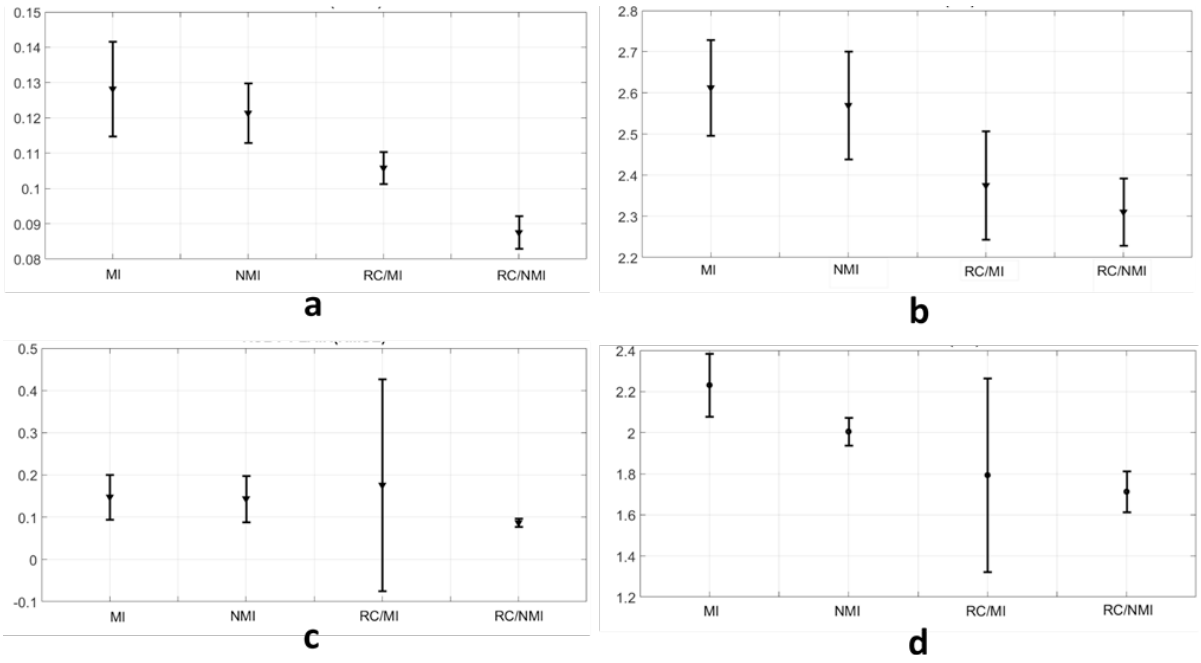

Figure 6. Error bar of metrics' performance registration between ADC map and rCBV map to FLAIR image, a) RMSE metric of ADC map to FLAIR image registration, b) HD metric of ADC map to FLAIR image registration, c) RMSE metric of rCBV map to FLAIR image registration, d) HD metric of rCBV map to FLAIR image registration.

4. Discussion

Our aim in this work was to increase the accuracy of multi-parametric MR image registration without increasing the computational complexity and to increase the robustness of the algorithm against noise and intensity inhomogeneity artifacts. Conventional SMs like MI and NMI induce incorrect results when images are aligned with each other. This is due to the sensitivity of these SMs to intensity inhomogeneity. As RC similarity measure tends to generate optimum results in correct alignment but has a lower capture range, when the differences between the two images are high, this method may fail. The key advantage of RC similarity measure relies in that it quantizes the residual complexity between the fixed and the floating image. In our work, we used DCT basis functions to show how complex is the residue image and we used *log(•)* to quantify this difference. DCT transforms the difference (residue) between the two images to a matrix filled with large numbers of zeroes. In this matrix, the elements representing a high difference among the two images have larger values.

Here, we showed that the combination of NMI with RC similarity measure being applied in multi-level image pyramid can effectively register multi-parametric images while compensating for noise and intensity inhomogeneity artifacts. The proposed registration framework performed better than typical similarity measures that have been employed in the literature. The multi-similarity measure was implemented in a multi-level manner in which, RC and NMI metrics were combined in different levels of wavelet decomposition. This approach outperformed the multi-level technique implemented using Gaussian decomposition method, as the latter blurs the images more than the former and causes the loss of structural details.

Nonetheless, our technique has been applied on a limited subject population and a further evaluation on larger number of patients is required for generalizing the results. Furthermore, the registration was performed in 2D which should be generalized to 3D registration technique in future works.

In conclusion, effective multi-parametric alignment of quantitative (ADC- and rCBV) maps to anatomical FLAIR images of glioma brain tumors can be achieved using 2D multi-level non-rigid registration technique with multi-

similarity (RC/NMI) measures. Furthermore, through the proposed approach, the capture range of multiparametric image registration algorithm and robustness against noise and intensity inhomogeneity artifacts could be improved.

References

1- A. Fathi Kazerooni *et al.*, "Characterization of active and infiltrative tumorous subregions from normal tissue in brain gliomas using multiparametric MRI," *Journal of Magnetic Resonance Imaging,* 2018.

2- A. F. Kazerooni *et al.*, "Segmentation of brain tumors in MRI images using multi-scale gradient vector flow," in *2011 Annual International Conference of the IEEE Engineering in Medicine and Biology Society*, 2011, pp. 7973-7976: IEEE.

3- A. F. Kazerooni, M. Mohseni, S. Rezaei, G. Bakhshandehpour, and H. S. Rad, "Multi-parametric (ADC/PWI/T2-w) image fusion approach for accurate semi-automatic segmentation of tumorous regions in glioblastoma multiforme," *Magnetic Resonance Materials in Physics, Biology and Medicine,* vol. 28, no. 1, pp. 13-22, 2015.

4- T. R. Jensen and K. M. Schmainda, "Computer-aided detection of brain tumor invasion using multiparametric MRI," *Journal of Magnetic Resonance Imaging,* vol. 30, no. 3, pp. 481-489, 2009.

5- S. Bauer, R. Wiest, L.-P. Nolte, and M. Reyes, "A survey of MRI-based medical image analysis for brain tumor studies," *Physics in Medicine & Biology,* vol. 58, no. 13, p. R97, 2013.

6- J. Čížek, K. Herholz, S. Vollmar, R. Schrader, J. Klein, and W.-D. Heiss, "Fast and robust registration of PET and MR images of human brain," *Neuroimage,* vol. 22, no. 1, pp. 434-442, 2004.

7- A. Mang *et al.*, "Registration of RCBV and ADC maps with structural and physiological MR images in glioma patients: Study and validation," in *Biomedical Imaging: From Nano to Macro, 2007. ISBI 2007. 4th IEEE International Symposium on*, 2007, pp. 37-40: IEEE.

8- J. Wu and A. C. Chung, "Multimodal brain image registration based on wavelet transform using SAD and MI," in *Medical Imaging and Augmented Reality*: Springer, 2004, pp. 270-277.

9- A. Myronenko and X. Song, "Intensity-based image registration by minimizing residual complexity," *Medical Imaging, IEEE Transactions on,* vol. 29, no. 11, pp. 1882-1891, 2010.

10- L. G. Brown, "A survey of image registration techniques," *ACM computing surveys (CSUR),* vol. 24, no. 4, pp. 325-376, 1992.

11- J. Modersitzki, *FAIR: flexible algorithms for image registration*. SIAM, 2009.

12- J. Modersitzki, *Numerical methods for image registration*. Oxford university press, 2003.

13- M. Holden, "A review of geometric transformations for nonrigid body registration," *Medical Imaging, IEEE Transactions on,* vol. 27, no. 1, pp. 111-128, 2008.

14- R. B. Tennakoon, A. Bab-Hadiashar, Z. Cao, and M. de Bruijne, "Nonrigid registration of volumetric images using ranked order statistics," *Medical Imaging, IEEE Transactions on,* vol. 33, no. 2, pp. 422-432, 2014.

15- P. Viola and W. M. Wells III, "Alignment by maximization of mutual information," *International journal of computer vision,* vol. 24, no. 2, pp. 137-154, 1997.

16- A. Collignon, F. Maes, D. Delaere, D. Vandermeulen, P. Suetens, and G. Marchal, "Automated multi-modality image registration based on information theory," in *Information processing in medical imaging*, 1995, vol. 3, no. 6, pp. 263-274.

17- A. Myronenko, "Non-rigid image registration regularization, algorithms and applications," 2010.

18- D. Rueckert, L. I. Sonoda, C. Hayes, D. L. Hill, M. O. Leach, and D. J. Hawkes, "Nonrigid registration using free-form deformations: application to breast MR images," *Medical Imaging, IEEE Transactions on,* vol. 18, no. 8, pp. 712-721, 1999.

19- M. Unser, "Splines: A perfect fit for signal and image processing," *Signal Processing Magazine, IEEE,* vol. 16, no. 6, pp. 22-38, 1999.

20- M. Unser, A. Aldroubi, and M. Eden, "B-spline signal processing. I. Theory," *Signal Processing, IEEE Transactions on,* vol. 41, no. 2, pp. 821-833, 1993.

21- R. C. Gonzalez and R. E. Woods, "Digital image processing," ed: Prentice hall Upper Saddle River, 2002.

22- A. F. Kazerooni, A. Ahmadian, H. Saberi, J. Alirezaie, and H. S. Rad, "An efficient algorithm for registration of pre-and intra-operative brain MRI images to correct intensity inhomogeneity," in *Information Science, Signal Processing and their Applications (ISSPA), 2012 11th International Conference on*, 2012, pp. 253-258: IEEE.

23- C. Studholme, D. L. Hill, and D. J. Hawkes, "An overlap invariant entropy measure of 3D medical

image alignment," *Pattern recognition,* vol. 32, no. 1, pp. 71-86, 1999.

24- J. V. Hajnal, D. L. Hill, and D. J. Hawkes, "Medical image registration," *CRC, Boca Raton,* 2001.

25- D. Rueckert, L. I. Sonoda, C. Hayes, D. L. Hill, M. O. Leach, and D. J. Hawkes, "Nonrigid registration using free-form deformations: application to breast MR images," *IEEE transactions on medical imaging,* vol. 18, no. 8, pp. 712-721, 1999.

26- J. Nocedal and S. Wright, *Numerical optimization*. Springer Science & Business Media, 2006.

27- E. Gilleland, T. C. Lee, J. Halley Gotway, R. Bullock, and B. G. Brown, "Computationally efficient spatial forecast verification using Baddeley's delta image metric," *Monthly Weather Review,* vol. 136, no. 5, pp. 1747-1757, 2008.

28- D. P. Huttenlocher, G. A. Klanderman, and W. J. Rucklidge, "Comparing images using the Hausdorff distance," *Pattern Analysis and Machine Intelligence, IEEE Transactions on,* vol. 15, no. 9, pp. 850-863, 1993.

29- D. P. Huttenlocher, G. A. Klanderman, and W. J. Rucklidge, "Comparing images using the Hausdorff distance," *IEEE Transactions on pattern analysis and machine intelligence,* vol. 15, no. 9, pp. 850-863, 1993.

30- R. Varadhan, G. Karangelis, K. Krishnan, and S. Hui, "A framework for deformable image registration validation in radiotherapy clinical applications," *Journal of applied clinical medical physics/American College of Medical Physics,* vol. 14, no. 1, p. 4066, 2013.